Engineering Valley Polarization of Monolayer WS₂: A Physical Doping Approach

Shun Feng, Chunxiao Cong,* Satoru Konabe, Jing Zhang, Jingzhi Shang, Yu Chen, Chenji Zou, Bingchen Cao, Lishu Wu, Namphung Peimyoo, Baile Zhang, and Ting Yu*

The emerging field of valleytronics has boosted intensive interests in investigating and controlling valley polarized light emission of monolayer transition metal dichalcogenides (1L TMDs). However, so far, the effective control of valley polarization degree in monolayer TMDs semiconductors is mostly achieved at liquid helium cryogenic temperature (4.2 K), with the requirements of high magnetic field and on-resonance laser, which are of high cost and unwelcome for applications. To overcome this obstacle, it is depicted that by electrostatic and optical doping, even at temperatures far above liquid helium cryogenic temperature (80 K) and under off-resonance laser excitation, a competitive valley polarization degree of monolayer WS₂ can be achieved (more than threefold enhancement). The enhanced polarization is understood by a general doping dependent valley relaxation mechanism, which agrees well with the unified theory of carrier screening effects on intervalley scattering process. These results demonstrate that the tunability corresponds to an effective magnet field of ≈10 T at 4.2 K. This work not only serves as a reference to future valleytronic studies based on monolayer TMDs with various external or native carrier densities, but also provides an alternative approach toward enhanced polarization degree, which denotes an essential step toward practical valleytronic applications.

Layered transition-metal dichalcogenides (TMDs) semiconductors have been demonstrated to carry the spin-like degree of freedom known as valley pseudospin, which can be optically generated and detected via circularly polarized photoluminescence (PL) spectra.[1–4] In specific, this twofold valley degree of freedom (DOF) directly corresponds to the optical bandgap of $+K$ and $-K$ valley in the Brillouin zone.[5] Due to strong spin–orbit coupling and broken inversion symmetry, together with time-reversal symmetry, spin and valley DOFs are coupled in monolayer TMDs.[6] This property enables selectively pumping $+K$ ($-K$) valley with left (right) hand circular light excitations

to create an imbalanced carrier population between two valleys. Realizing such net valley polarization is an essential step for developing valleytronic devices.[7–11] Resulted from the opposite selection rules of two valleys, controlling valley polarization in mono-layer TMDs by optical helicity is achievable. As experimentally measured, the circular polarization degree (P_c) reflects the population ratio between two valleys which generate light emissions with opposite helicity. Ideally, if photoexcited carriers are fully polarized within single valley, this value should be approaching 100%. However, the reported values of P_c in monolayer TMDs vary from 2% to nearly 100% among different TMD semiconductors,[12–16] which are mainly attributed to intervalley scattering process from the selectively pumped valley to the opposite one.[16–18] As for the PL measurements, various approaches have been adopted to obtain a sizable P_c like applying magnetic field, cooling down to liquid helium cryogenic temperature, using near resonant light excitation or building van der Waals heterostructure.[1,3,12,19–24] More practical and desirable methods could be electrical and optical control of valley polarization in TMDs at noncryogenic temperature and off-resonance conditions. Toward this goal, one of the most effective means is in situ carrier doping by physical or chemical approaches.[25–27] The introduced resident carriers in TMDs not only tailor the exciton species, but are expected to considerably tune the valley polarization dynamics which dominates P_c values as well. In previous reports, the changes of valley polarization/relaxation dynamics due to carrier doping

S. Feng, Dr. J. Zhang, J. Z. Shang, Dr. Y. Chen, Dr. C. J. Zou, Dr. B. C. Cao, L. S. Wu, Dr. N. Peimyoo, Prof. B. L. Zhang, Prof. T. Yu
Division of Physics and Applied Physics
School of Physical and Mathematical Sciences
Nanyang Technological University
637371 Singapore, Singapore
E-mail: yuting@ntu.edu.sg

(iD) The ORCID identification number(s) for the author(s) of this article can be found under https://doi.org/10.1002/smll.201805503.

Prof. C. X. Cong
State Key Laboratory of ASIC & System
School of Information Science and Technology
Fudan University
Shanghai 200433, China
E-mail: cxcong@fudan.edu.cn

Prof. S. Konabe
Department of Chemical Science and Technology
Hosei University
Koganei Tokyo 184-8584, Japan

1805503 (1 of 7)

ADVANCED
SCIENCE NEWS
www.advancedsciencenews.com

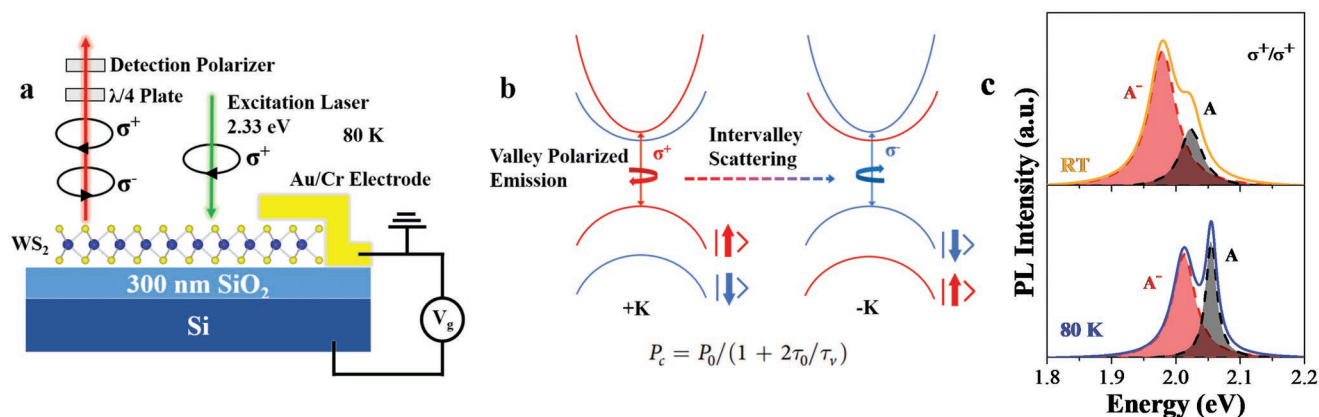NANO · MICRO
small
www.small-journal.com

Figure 1. Monolayer WS$_2$ based device to explore the doping dependent valley relaxation dynamics. Schematic image of: a) experimental set up for circularly polarized PL at various carrier densities, b) optical selection rules at $+K/-K$ valleys and intervalley scattering process. c) Polarization resolved PL spectra with σ^+/σ^+ configuration at room temperature and 80 K.

have been noticed but have not been investigated systematically and the mechanism remains elusive.[13,21,28,29] In addition, the unintentional doping and localized states in TMD samples play important roles to influence their optical properties, which may lead to discrepancies in experiments using layered TMD samples with different initial electronic states.[30,31] Therefore, probing correlations between valley polarization and carrier concentration is crucial for future manipulations and potential applications based on valleytronic properties in TMD samples prepared by mechanical exfoliation or chemical vapor deposition (CVD) with various native and/or external carrier doping from environment and laser excitation.

Inspired by a recent theoretical study together with an experimentally proved framework based on carrier screening effects on excitonic valley relaxation in 2D semiconductors,[32,33] here we designed a strategy to greatly enhance P_c at liquid nitrogen temperature. Doping dependent circularly polarized PL spectra of monolayer WS$_2$ at temperature of 80 K under off-resonance excitation (2.33 eV) are studied. The carrier density of the sample is controlled by electrostatic and optical doping. The evolution of neutral and charged exciton emission states have been extracted. Surprisingly the electrostatic doping drives continuous increase of P_c for charged exciton emission. Besides, by controlling photoexcitation strength, a considerable modulation of polarization degree is also depicted, parallel with the electrical doping effects. By comparing these findings with a general doping dependent valley relaxation mechanism and previous reports on exciton dynamics, we reveal the correlation between P_c and physical doping. Our results demonstrate the tunable valley polarization degree under low cost and helium-free condition, equally effective as conducted under 10 T magnetic field.[34] We successfully enriched the understanding of valley relaxation process by electrostatic and optical doping means, which denotes an essential step toward practical valleytronic applications.

Polarization-resolved PL measurements of the mechanically exfoliated monolayer WS$_2$ were conducted under excitation from a σ^+ circular polarized 532 nm (2.33 eV) laser and filtered with σ^+/σ^- helicity to measure the emission from $+K/-K$ valley

(**Figure 1**a). The polarization degree P_c is calculated by the equation

$$P_c = \frac{I(\sigma^+) - I(\sigma^-)}{I(\sigma^+) + I(\sigma^-)} \tag{1}$$

where $I(\sigma^+)/I(\sigma^-)$ denotes the left/right hand circular polarization resolved PL intensity. Based on optical selection rule, σ^+ (σ^-) excitation solely couples to excitonic transitions in the $+K$ ($-K$) valley and the corresponding light emission should carry single handedness. However, as schematically shown in Figure 1b, when the $+K$ valley is selectively pumped with σ^+ excitation, the resulted PL light emission contain not only σ^+ signal from polarized excitonic transitions in $+K$ valley but also σ^- signal due to intervalley scattering of excitons from $+K$ to $-K$ valley.[18] The overall circular polarization degree P_c is determined by equation

$$P_c = P_0/(1 + 2\tau_0/\tau_v) \tag{2}$$

where P_0 is initial polarization, τ_0 is the valley exciton decay time, and τ_v is the intervalley relaxation time. The term τ_0/τ_v indicates that the value of P_c largely depends on the competition between two processes: radiative recombination of valley polarized excitons ($\approx \tau_0$) and intervalley scattering ($\approx \tau_v$). While τ_v (intervalley scattering dynamics) can be significantly tuned by screening effect induced by carrier doping, which will be discussed in detail later. Figure 1c shows PL spectra from a field effect device of exfoliated 1L-WS$_2$ measured at room temperature (RT) and 80 K. Generally, the PL spectra consists of two components, where the high/low energy peak corresponds to neutral exciton (A)/negative trion (A^-) emission.[26] At low temperature the A and A^- peaks present a blue shift which has also been observed in exfoliated MoS$_2$, MoSe$_2$ and chemical vapor deposited WS$_2$ recently.[35,36] The two exciton peaks are well resolved at various carrier concentration, which enable us to perform the multiple-peak fitting properly and study the evolution of these two exciton species separately.

First part of the article is the results of physical doping induced polarization enhancement. **Figure 2**a shows PL
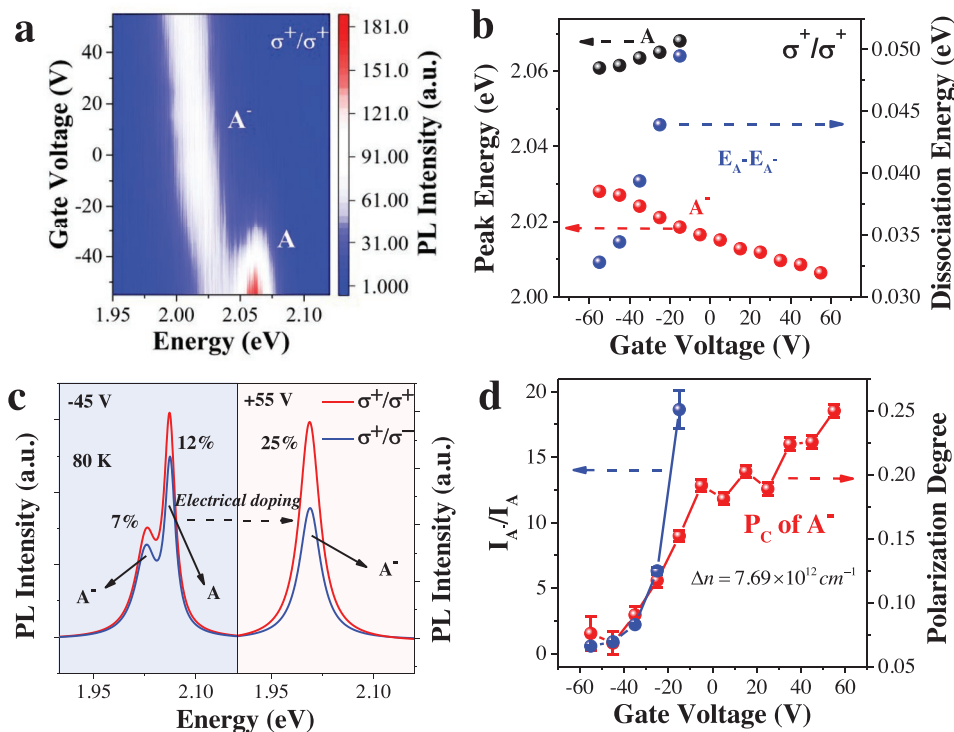
**ADVANCED
SCIENCE NEWS**
www.advancedsciencenews.com

**NANO · MICRO
small**
www.small-journal.com

Figure 2. Gate voltage dependent circularly polarized PL measurement of monolayer WS_2 at 80 K. All optical excitation is left circularly polarized (σ^+). The exciton species and corresponded polarization degree values are labeled, respectively. a) PL intensity mapping (color scale in counts) of monolayer WS_2 as a function of gate voltage and photon energy, with σ^+ detection. b) Corresponding Photon energies of A and A^- excitons (left vertical axis) and dissociation energy of A^- (right vertical axis) versus gate voltage. c) Polarization resolved PL spectra of gated WS_2, both with σ^+ (σ^-) detection at 80 K. d) Intensity ratios I_{A^-}/I_A (left vertical axis) and A^- circular polarization degree (left vertical axis) measured in as-exfoliated 1L WS_2 versus gate voltage. The error bars correspond to standard errors of peak heights in multiple-peak fittings.

features from a field effect device of exfoliated 1L-WS_2 with the back-gate voltages from −55 to 55 V at 80 K. Overall, two components A and A^- emission band are well identified. Their corresponding photon energies and spectra dominance change as the voltage sweeps. At gate voltage below −15 V, both A and A^- features are visible. While at higher gate voltage, the integrated intensity of A peak gradually decreases and A^- peak becomes dominated due to the electrostatic doping, resulting in a single peak profile at higher carrier density. In addition, the peak position of A blueshifts and that of A^- redshifts, which leads to the increase of energy difference between A and A^- (i.e., dissociation energy), as can be directly seen in Figure 2b. This is attributed to phase space blocking due to Pauli exclusion and many body effects.[37] As the gate voltage sweeps from negative to positive, the A^- emission energy redshifts by roughly 21 meV. The dissociation energy also monotonically increases to around 50 meV from gate voltage of −55 to −15 V. These behaviors agree well with the previous experimental reports on natively N-doped TMDs like MoS_2 and WS_2.[26,38,39] The maximum external doping level is estimated as $\Delta n = 7.69 \times 10^{12}$ cm^{-2} at 55 V gate voltage compared with −55 V (Section S1, Supporting Information).

Helicity resolved PL spectra from P-type (−45 V) and N-type (+55 V) gated sample are shown in Figure 2c. When the WS_2 is negatively gated, A^- shows a low polarization degree of 7%. While, at a positive gate voltage and a higher induced carrier

density, the sample exhibits a single A^- peak and a drastically higher polarization degree of 25%. The evolution of polarization degree as a function of gate voltages is shown in Figure 2d. As an indicator of the electron density, the integrated intensity ratio of A^- to A is illustrated at lower carrier concentration regime where the neutral exciton A is visible. The increment of this ratio indicates elevated electron density.[30,40,41] Obviously, as the voltage is swept from −55 to +55 V, the polarization of trion is enhanced by more than threefold. Compared to the previous reports,[14,42] the overall P_c value especially at lower doping level is relatively low, potentially attributed to a large detuning energy ≈0.3 eV caused by the off-resonance laser excitation and a temperature far above typical helium cryogenic temperature (4–10 K), which leads to lower initial polarization (P_0).[18,43] More detailed discussion of P_0 is shown in following parts.

As reported in graphene[44] and TMDs,[26] in addition to electrostatic doping, the carrier concentration can also be modified by light excitation, which not only creates electron–hole pairs, but dynamically ionizes the carriers trapped on the donor impurities levels toward conduction band as well.[45] Here, we studied the influence of excitation laser power on the circularly polarized PL emission of 1L WS_2 at 80 K. **Figure 3**a shows the intensity mapping of PL spectra at various excitation power, in σ^+/σ^+ configuration. Like electrostatic doping case, the overall PL profile evolves from the two-peak
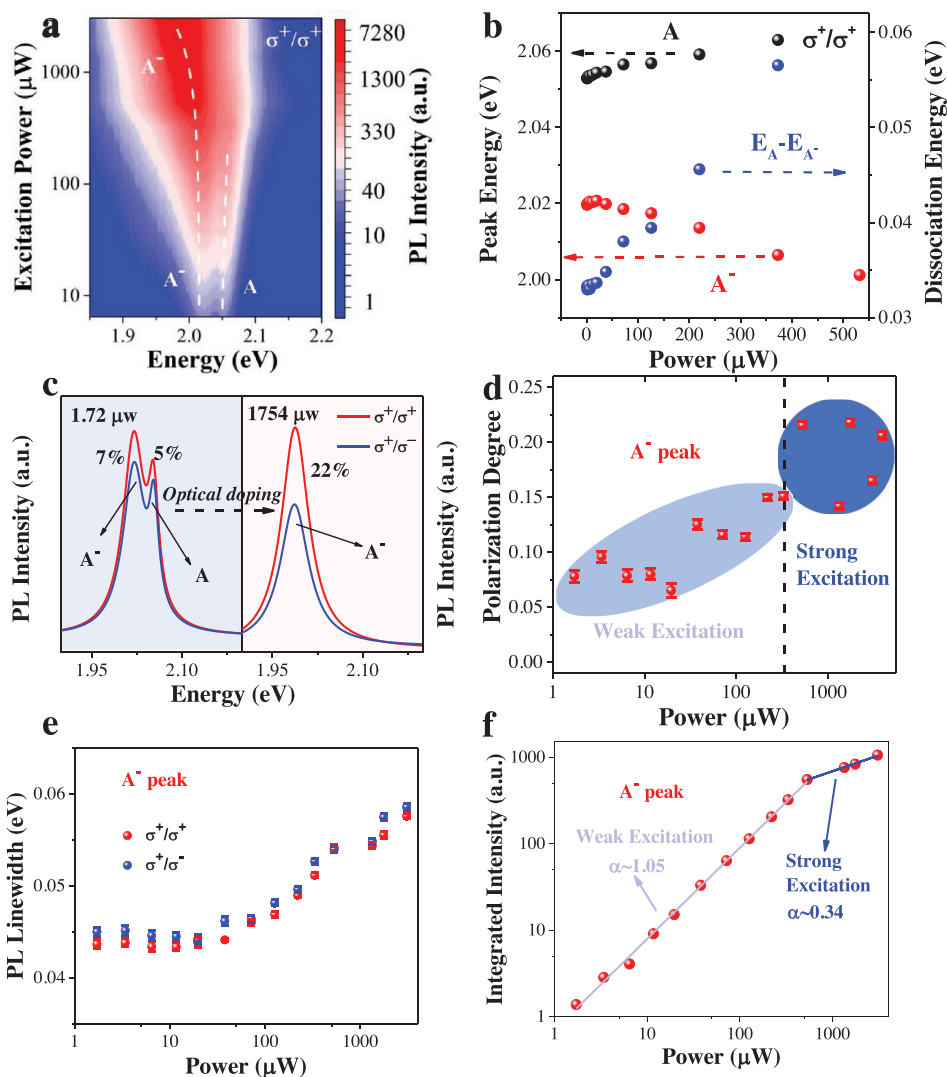
Figure 3. Power dependent circularly polarized PL measurement of monolayer WS_2 at 80 K. a) PL intensity mapping (color in counts) of monolayer WS_2 as a function of excitation power and photon energy, with σ^+ detection. Note that the intensity and power are in log scale. b) Corresponding photon energies of A and A^- excitons (left vertical axis) and dissociation energy of A^- (right vertical axis) versus power. c) Polarization resolved PL spectra of WS_2 pumped at different powers. d) Circular polarization degree, e) A^- linewidth and f) integrated intensity of trion peak measured in 1L WS_2 at various excitation power. Solid lines are linear fitting curves on log–log scales and α values correspond to the slopes. The error bars correspond to standard errors of peak heights/widths in multiple-peak fittings.

(A and A^-) feature into a single peak (A^-) feature at increasing excitation powers. The corresponding photon energies and integrated intensities versus power are depicted in Figure 3b. Identical to electrostatic doping case, as power increases within 600 µW, the A exciton peak slightly blueshifts while the A^- exciton peak redshifts, which are signatures of photoinduced electron doping.[13,26,43]

With regards to the optical doping dependent valley polarization, as shown in Figure 3c, the P_c value of A^- shows great distinction at 1.72 µW (or 0.219 kW cm^{-2}) and 1754 µW (or 223.32 kW cm^{-2}) excitation. The corresponding power density at sample surface is calculated in Figure S6 in the Supporting Information. In details, threefold enhancement of P_c from 7% to 22% is achieved with power increasing from 1.72 µW (or 0.219 kW cm^{-2}) to 3930 mW (or 500.38 kW cm^{-2}). The

completed power dependence of P_c is plotted in Figure 3d. Compared to the gate voltage dependence, there is pronounced fluctuation rather than mono-tonous increasing, especially at higher powers in mW scale. At both low and high powers, the carrier doping induced screening effect is prominent to influence valley polarization.

Second part of the article is the discussion of mechanism for polarization enhancement. For both electrostatic and optical doping cases, the enhancement of valley polarization obtained in this work is mainly attributed to carrier doping induced suppression on valley relaxation process. The intervalley scattering process of exciton is governed by electron–hole exchange interaction through the Maialle–Silva–Sham mechanism, resulting in short valley lifetime in picosecond scale.[46–48] In the previous studies by electrically tailoring the doping states in graphene,

the intervalley scattering rate was strongly suppressed.[49] This carrier doping approach was proposed to be applicable to other multivalley systems like TMDs. Furthermore, as indicated by a comprehensive theoretical study on WS$_2$ recently,[32] intervalley exciton relaxation time (τ_v) correlates with carrier concentrations and temperatures. This framework is quantitatively compared with our experiment results. In this work we are trying to manipulate the τ_0/τ_v value by tuning electron doping and then to tailor the P_c value consequently. In regards of the electron doping effect on τ_v, the previous mentioned framework suggests in both collisional and thermal broadening regimes, the value of τ_v shows maximum discrepancy (approximately sixfold) versus carrier concentration at around 70–90 K.[32] This implies the intervalley scattering process can be effectively suppressed by carrier doping at liquid nitrogen temperature (i.e., 80 K). Compared to τ_v, τ_0 is much less affected by carrier doping, supported by stable linewidth and integrated intensities upon doping,[41,50] as discussed in Section S3 (Figure S1, Supporting Information). Consequently, the τ_0/τ_v and P_c values are considerably tuned by electrostatic doping, which agrees well with our experimental observations. This is of great importance for the circularly polarized PL study at liquid nitrogen temperature. The physical doping effect is further illustrated by following experiments.

For the optical doping, at low optical excitation (<532 μW, corresponding to 67.73 kW cm^{-2}), the overall effect of photo induced electron doping is clearly demonstrated, which is comparable to our observation in the gate dependent PL measurements. In details, it is noticed that the dissociation energy between A and A^- at various power shift in the same manner as the electrostatic gated sample. Under the excitation of 373 μW (or 47.49 kW cm^{-2}), the observed dissociation energy is as large as around 0.05 eV, equivalent to doping effect of 40 V voltage difference (from −55 to −15 V) and electron density increase is estimated as 2.79×10^{12} cm^{-2}. Importantly, the electron doping effect on valley relaxation is witnessed in the evolution of P_c values. In this regime the P_c value is increased from 7% to 15%. This twofold enhancement stay in line with our electrical doping results within 50 V difference and indicates the τ_0/τ_v is effectively tailored.

At higher powers from 532 to 3930 μW (67.73 to 500.38 kW cm^{-2}), however, the P_c value become more diverged with a weak increasing trend up to 22% at 1754 μW (or 223.32 kW cm^{-2}). The power dependence of A^- integrated intensity ($I_{Total} = I_{\sigma^+} + I_{\sigma^-}$) is depicted in Figure 3f. The intensity shows linear relationship with excitation power and a slope of ≈1.05 at power less than 532 μW then saturated with a slope of 0.34. This first slope value presents a symbol of A and A^- exciton emission.[13,26] Noticeably, at higher power the A^- peak experiences obvious broadening from 44 to 57 meV caused by excitation induced dephasing effect (Figure 3e).[52] This is in sharp contrast with the electrical doping case where the A^- exciton linewidth is relatively unchanged at various gate voltages (Figure S1c, Supporting Information). Note that the excitonic linewidth is a partial reflector of the coherence lifetime, which is influenced by intervalley scattering.[51,52] Theoretically, this PL linewidth is proved to be inversely proportional to the τ_v term when temperature and doping level are fixed (Section S2, Supporting Information).[32,33] As consequences from accelerated intervalley scattering, excitation induced broadening indicates

that the further increment of τ_v is hampered. It compromises the enhancement of P_c compared to electrostatic doping case at similar electron density. We applied previous mentioned framework to estimate the P_c with different electron density and PL peak width and obtained reasonable results which agree well with the experimental data range (Section S2, Supporting Information). Other potential effects like many body effects[53,54] and intravalley depolarization are also discussed (Section S3, Supporting Information), which are not the focus of this article. Overall, these results indicate a threefold enhancement of P_c by pure optical excitation, without requirement for device fabrication. Our findings also serve as a reference to the future TMDs based valley polarized PL or photodetector[10] studies conducted at different excitation powers.

Unlike the ideal case,[6] P_0 is less than 1 due to defect assisted exciton trapping[55] and ultrafast relaxation of hot excitons,[56] and worth for more detailed discussion. The value of P_0 is mainly dependent on the detuning energy, which is the energy difference between excitation laser and A exciton emission.[16,18,57,58] It is worth noting that the possibility of P_c enhancement being determined by the change of detuning energy is ruled out, because as the electrical/optical doping increases, the A^- emission energy goes through red shift, which enlarges the detuning energy and may slightly reduce P_c rather than increases it.[16,17] In regards of the P_0 value, while some studies treated P_0 as 1 for simplicity,[59] previous time resolved PL has measured $P_0 = 0.7 \pm 0.1$ in monolayer WSe$_2$ system with around 150 meV detuning energy.[33] As has been theoretically pointed out,[32] the change of τ_v is around six times at 80 K when the carrier concentration is tuned from 8×10^{11} cm^{-2} to 8×10^{12} cm^{-2}, which relatively corresponds to our previously estimated doping state ($\Delta n = 7.69 \times 10^{12}$ cm^{-2}). We substitute the experimentally measured P_c and corresponding τ_0/τ_v values at low and high doping into Equation (1) to estimate the value of P_0, which is 51% (Section S2, Supporting Information). Due to the 300 meV detuning energy, the limited value below theoretical limit is consistent with the previous reports.[14,58] Though, via intentional doping, the measured valley polarization P_c can be engineered to approach P_0, yielding an acceptable value even under off-resonance excitation.

Last, we compare our results with the previous reports on tailoring P_c in exfoliated monolayer WS$_2$. Recent magneto-PL study has demonstrated valley Zeeman splitting and monotonically increasing P_c of A^- emission with applied magnet field in out of plane direction.[34] Compared to magnetic methods, electrical/optical control of valley states are more favored for future valleytronic devices operations. As a more practical method to create population imbalance between two valleys, our approaches correspond to a 10 T magnetic field which enhances polarization degree of trion emission from negligible value to about 25% at 4.2 K.[34] For PL without magnetic field, Cui et al. reported $P_c = 40\%$ at near resonance excitation (2.088 eV) and 16% at off-resonance excitation (2.331 eV), measured at 10 K. Korn and co-workers reported 21% for singlet trion and 34% for triplet trion with 2.15 eV laser excitation at 4.5 K.[42] It is clear that we boost the P_c of monolayer WS$_2$ to a decent value (25% for electrical doping, 22% for optical doping) comparable to the previous achieved ones with
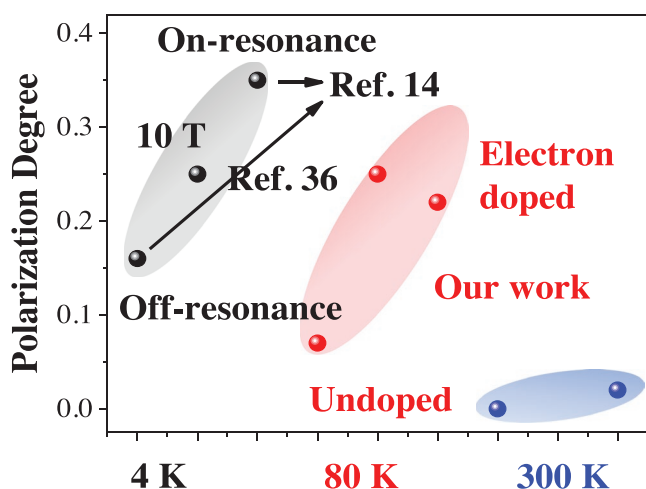
Figure 4. Comparison with previous report on circularly polarized PL measurement of monolayer WS_2. Black dots denote the previous reported P_c values in refs. [14] and [34]. Red (blue) dots represent P_c from our work with and without physical doping at 80 K (300 K).

much more demanding facilities (**Figure 4**). The gate voltage dependent circularly polarized PL at room temperature (300 K) is also performed (Figure S5, Supporting Information), the obtained P_c values are negligible without clear trend compared to the doping dependent data at 80 K. This is attributed to reduced τ_v[15] and suppressed tunability by electron doping[32] at higher temperature range.

In summary, we have studied the valley polarized excitonic emission of monolayer WS_2. By changing the gate voltage and the excitation power, doping tunable polarization degree in trion emission is achieved. The correlation between electron doping, exciton linewidth and valley polarization are clearly demonstrated in our measurements. In electrical doping case the increasing is mainly attributed to doping induced screening effect, while in optical doping case, especially at higher excitation powers in mW scale, not only the screening but also excitation induced perturbation is needed to be taken into considerations to explain the spectra features and P_c evolution. These findings serve as a reference for future valleytronic studies using TMD samples with different native or extrinsic doping level. Furthermore, based on our discovery of carrier screening effect, chemical doping or heterostructure formation are also expected to affect the valley polarization of A excitons in TMDs, which is promising for nondegenerated P_c engineering. Such enhanced polarization degree could provide additional degrees of freedom in realizing valley polarized exciton condensation,[60] exciton–polariton emission[61,62] and polariton fluid transport.[63] Our studies develop a simple but practical strategy for electrical and optical control of the valley polarization state, which is a corner stone for future noncryogenic valleytronic operations.

Experimental Section

Sample Preparation and Device Fabrication: Commercial WS_2 crystal (2D semiconductors Inc.) was mechanically exfoliated onto highly doped 300 nm thick SiO_2/Si wafer. For the device fabrication, the drain/source electrodes were made of 5/80 nm of Cr/Au by thermal evaporation and

after standard electron beam lithography (Oxford SEM system) and the lift-off process. Before the gated PL measurements, the device was wire bonded to a printed circuit board (PCB).

Photoluminescence Spectroscopy: Micro-PL measurements were performed using a WITec Raman system with excitation wavelengths of 532 nm through 50× objective lens (1.2 µm laser spot). As for the circular polarization resolved PL, a quarter wave plate was inserted along incident light to convert the linear polarized laser into circular polarized light. Besides a linear polarizer was inserted along the emission light before CCD collection to filter the emission light with left/right helicities. Grating (600 lines mm^{-1}) was used for PL measurements. For gate-dependent PL measurement the sample was loaded in the Linkam stage and connected with a Keithley 4200-SCS semiconductor characterization system to apply gate voltage between Si substrate and the source/drain electrode, at 80 K in high vacuum (10^{-3} mbar). The excitation power was kept at 40 µW (5.09 kW cm^{-2}) for gate dependent circularly polarized PL measurement. The sample size is generally larger than 5 µm for exfoliated monolayer which is larger than laser spot area. Among different samples, the smooth monolayer region was chosen at the center of flake to avoid the effect of edge states or metal contacts. Therefore, the difference of pumping/detecting area is minimal among different samples. The accuracy of the circular polarization degree for our setup was no less than 92.0%.

Supporting Information

Supporting Information is available from the Wiley Online Library or from the author.

Conflict of Interest

The authors declare no conflict of interest.

[1] K. F. Mak, K. He, J. Shan, T. F. Heinz, *Nat. Nanotechnol.* **2012**, *7*, 494.

[2] T. Cao, G. Wang, W. Han, H. Ye, C. Zhu, J. Shi, Q. Niu, P. Tan, E. Wang, B. Liu, J. Feng, *Nat. Commun.* **2012**, *3*, 887.

[3] H. Zeng, J. Dai, W. Yao, D. Xiao, X. Cui, *Nat. Nanotechnol.* **2012**, *7*, 490.

[4] X. Xu, W. Yao, D. Xiao, T. F. Heinz, *Nat. Phys.* **2014**, *10*, 343.

[5] K. F. Mak, C. Lee, J. Hone, J. Shan, T. F. Heinz, *Phys. Rev. Lett.* **2010**, *105*, 136805.

ADVANCED
SCIENCE NEWS
www.advancedsciencenews.com

NANO · MICRO
small
www.small-journal.com

[6] D. Xiao, G.-B. Liu, W. Feng, X. Xu, W. Yao, *Phys. Rev. Lett.* **2012**, *108*. 196802.

[7] D. Xiao, W. Yao, Q. Niu, *Phys. Rev. Lett.* **2007**, *99*, 236809.

[8] A. Rycerz, J. Tworzydło, C. W. J. Beenakker, *Nat. Phys.* **2007**, *3*, 172.

[9] W. Yao, D. Xiao, Q. Niu, *Phys. Rev. B* **2008**, *77*, 235406.

[10] M. Eginligil, B. Cao, Z. Wang, X. Shen, C. Cong, J. Shang, C. Soci, T. Yu, *Nat. Commun.* **2015**, *6*, 7636.

[11] W. Yang, J. Shang, J. Wang, X. Shen, B. Cao, N. Peimyoo, C. Zou, Y. Chen, Y. Wang, C. Cong, *Nano Lett.* **2016**, *16*, 1560.

[12] G. Sallen, L. Bouet, X. Marie, G. Wang, C. R. Zhu, W. P. Han, Y. Lu, P. H. Tan, T. Amand, B. L. Liu, B. Urbaszek, *Phys. Rev. B* **2012**, *86*, 081301.

[13] G. Plechinger, P. Nagler, J. Kraus, N. Paradiso, C. Strunk, C. Schüller, T. Korn, *Phys. Status Solidi RRL* **2015**, *9*, 457.

[14] B. Zhu, H. Zeng, J. Dai, Z. Gong, X. Cui, *Proc. Natl. Acad. Sci. USA* **2014**, *111*, 11606.

[15] A. T. Hanbicki, G. Kioseoglou, M. Currie, C. S. Hellberg, K. M. McCreary, A. L. Friedman, B. T. Jonker, *Sci. Rep.* **2016**, *6*, 18885.

[16] G. Kioseoglou, A. T. Hanbicki, M. Currie, A. L. Friedman, B. T. Jonker, *Sci. Rep.* **2016**, *6*, 25041.

[17] T. Yan, X. Qiao, P. Tan, X. Zhang, *Sci. Rep.* **2015**, *5*, 15625.

[18] G. Kioseoglou, A. T. Hanbicki, M. Currie, A. L. Friedman, D. Gunlycke, B. T. Jonker, *Appl. Phys. Lett.* **2012**, *101*, 221907.

[19] Y. Li, J. Ludwig, T. Low, A. Chernikov, X. Cui, G. Arefe, Y. D. Kim, A. M. van der Zande, A. Rigosi, H. M. Hill, S. H. Kim, J. Hone, Z. Li, D. Smirnov, T. F. Heinz, *Phys. Rev. Lett.* **2014**, *113*, 266804.

[20] A. Srivastava, M. Sidler, A. V. Allain, D. S. Lembke, A. Kis, A. Imamoglu, *Nat. Phys.* **2015**, *11*, 141.

[21] A. T. Hanbicki, K. M. McCreary, G. Kioseoglou, M. Currie, C. S. Hellberg, A. L. Friedman, B. T. Jonker, *AIP Adv.* **2016**, *6*, 055804.

[22] L. Du, Q. Zhang, B. Gong, M. Liao, J. Zhu, H. Yu, R. He, K. Liu, R. Yang, D. Shi, *Phys. Rev. B* **2018**, *97*, 115445.

[23] F. Cadiz, E. Courtade, C. Robert, G. Wang, Y. Shen, H. Cai, T. Taniguchi, K. Watanabe, H. Carrere, D. Lagarde, *Phys. Rev. X* **2017**, *7*, 021026.

[24] A. Arora, R. Schmidt, R. Schneider, M. R. Molas, I. Breslavetz, M. Potemski, R. Bratschitsch, *Nano Lett.* **2016**, *16*, 3624.

[25] N. Peimyoo, W. Yang, J. Shang, X. Shen, Y. Wang, T. Yu, *ACS Nano* **2014**, *8*, 11320.

[26] J. Shang, X. Shen, C. Cong, N. Peimyoo, B. Cao, M. Eginligil, T. Yu, *ACS Nano* **2015**, *9*, 647.

[27] S. Feng, C. Cong, N. Peimyoo, Y. Chen, J. Shang, C. Zou, B. Cao, L. Wu, J. Zhang, M. Eginligil, X. Wang, Q. Xiong, A. Ananthanarayanan, P. Chen, B. Zhang, T. Yu, *Nano Res.* **2018**, *11*, 1744.

[28] A. M. Jones, H. Yu, N. J. Ghimire, S. Wu, G. Aivazian, J. S. Ross, B. Zhao, J. Yan, D. G. Mandrus, D. Xiao, W. Yao, X. Xu, *Nat. Nanotechnol.* **2013**, *8*, 634.

[29] P. Dey, L. Yang, C. Robert, G. Wang, B. Urbaszek, X. Marie, S. A. Crooker, *Phys. Rev. Lett.* **2017**, *119*, 137401.

[30] J. Shang, C. Cong, X. Shen, W. Yang, C. Zou, N. Peimyoo, B. Cao, M. Eginligil, W. Lin, W. Huang, *Phys. Rev. Mater.* **2017**, *1*, 074001.

[31] C. Cong, J. Shang, X. Wu, B. Cao, N. Peimyoo, C. Qiu, L. Sun, T. Yu, *Adv. Opt. Mater.* **2014**, *2*, 131.

[32] S. Konabe, *Appl. Phys. Lett.* **2016**, *109*, 073104.

[33] Y. Miyauchi, S. Konabe, F. Wang, W. Zhang, A. Hwang, Y. Hasegawa, L. Zhou, S. Mouri, M. Toh, G. Eda, *Nat. Commun.* **2018**, *9*, 2598.

[34] G. Plechinger, P. Nagler, A. Arora, A. Granados del Águila, M. V. Ballottin, T. Frank, P. Steinleitner, M. Gmitra, J. Fabian, P. C. Christianen, *Nano Lett.* **2016**, *16*, 7899.

[35] S. Tongay, J. Zhou, C. Ataca, K. Lo, T. S. Matthews, J. Li, J. C. Grossman, J. Wu, *Nano Lett.* **2012**, *12*, 5576.

[36] N. Peimyoo, J. Shang, C. Cong, X. Shen, X. Wu, E. K. Yeow, T. Yu, *ACS Nano* **2013**, *7*, 10985.

[37] C. Zhang, H. Wang, W. Chan, C. Manolatou, F. Rana, *Phys. Rev. B* **2014**, *89*, 205436.

[38] K. F. Mak, K. He, C. Lee, G. H. Lee, J. Hone, T. F. Heinz, J. Shan, *Nat. Mater.* **2013**, *12*, 207.

[39] B. Zhu, X. Chen, X. Cui, *Sci. Rep.* **2015**, *5*, 9218.

[40] J. S. Ross, S. Wu, H. Yu, N. J. Ghimire, A. M. Jones, G. Aivazian, J. Yan, D. G. Mandrus, D. Xiao, W. Yao, X. Xu, *Nat. Commun.* **2013**, *4*, 1474.

[41] S. Mouri, Y. Miyauchi, K. Matsuda, *Nano Lett.* **2013**, *13*, 5944.

[42] G. Plechinger, P. Nagler, A. Arora, R. Schmidt, A. Chernikov, A. G. del Águila, P. C. M. Christianen, R. Bratschitsch, C. Schüller, T. Korn, *Nat. Commun.* **2016**, *7*, 12715.

[43] K. M. McCreary, M. Currie, A. T. Hanbicki, H. J. Chuang, B. T. Jonker, *ACS Nano* **2017**, *11*, 7988.

[44] L. Ju, J. Velasco Jr., E. Huang, S. Kahn, C. Nosiglia, H.-Z. Tsai, W. Yang, T. Taniguchi, K. Watanabe, Y. Zhang, G. Zhang, M. Crommie, A. Zettl, F. Wang, *Nat. Nanotechnol.* **2014**, *9*, 348.

[45] A. Mitioglu, P. Plochocka, J. Jadczak, W. Escoffier, G. Rikken, L. Kulyuk, D. Maude, *Phys. Rev. B* **2013**, *88*, 245403.

[46] M. Z. Maialle, E. A. de Andrada e Silva, L. J. Sham, *Phys. Rev. B* **1993**, *47*, 15776.

[47] C. Mai, A. Barrette, Y. Yu, Y. G. Semenov, K. W. Kim, L. Cao, K. Gundogdu, *Nano Lett.* **2014**, *14*, 202.

[48] X. Song, S. Xie, K. Kang, J. Park, V. Sih, *Nano Lett.* **2016**, *16*, 5010.

[49] B. Yan, Q. Han, Z. Jia, J. Niu, T. Cai, D. Yu, X. Wu, *Phys. Rev. B* **2016**, *93*, 041407.

[50] H. Wang, C. Zhang, W. Chan, C. Manolatou, S. Tiwari, F. Rana, *Phys. Rev. B* **2016**, *93*, 045407.

[51] M. Selig, G. Berghäuser, A. Raja, P. Nagler, C. Schüller, T. F. Heinz, T. Korn, A. Chernikov, E. Malic, A. Knorr, *Nat. Commun.* **2016**, *7*, 13279.

[52] G. Moody, C. K. Dass, K. Hao, C.-H. Chen, L.-J. Li, A. Singh, K. Tran, G. Clark, X. Xu, G. Berghäuser, *Nat. Commun.* **2015**, *6*. 8315.

[53] Y. Yu, Y. Yu, C. Xu, A. Barrette, K. Gundogdu, L. Cao, *Phys. Rev. B* **2016**, *93*, 2011156.

[54] L. Yuan, L. Huang, *Nanoscale* **2015**, *7*, 7402.

[55] Q. Wang, S. Ge, X. Li, J. Qiu, Y. Ji, J. Feng, D. Sun, *ACS Nano* **2013**, *7*, 11087.

[56] T. Yu, M. Wu, *Phys. Rev. B* **2014**, *89*, 205303.

[57] B. R. Carvalho, Y. Wang, S. Mignuzzi, D. Roy, M. Terrones, C. Fantini, V. H. Crespi, L. M. Malard, M. A. Pimenta, *Nat. Commun.* **2017**, *8*, 14670.

[58] H. Su, A. Deng, Z. Zhen, J.-F. Dai, *Phys. Rev. B* **2018**, *97*, 115426.

[59] P. K. Nayak, F.-C. Lin, C.-H. Yeh, J.-S. Huang, P.-W. Chiu, *Nanoscale* **2016**, *8*, 6035.

[60] A. Kogar, M. S. Rak, S. Vig, A. A. Husain, F. Flicker, Y. I. Joe, L. Venema, G. J. MacDougall, T. C. Chiang, E. Fradkin, J. van Wezel, P. Abbamonte, *Science* **2017**, *358*, 1314.

[61] T. Byrnes, N. Y. Kim, Y. Yamamoto, *Nat. Phys.* **2014**, *10*, 803.

[62] Z. Sun, J. Gu, A. Ghazaryan, Z. Shotan, C. R. Considine, M. Dollar, B. Chakraborty, X. Liu, P. Ghaemi, S. Kéna-Cohen, V. M. Menon, *Nat. Photonics* **2017**, *11*, 491.

[63] F. Barachati, A. Fieramosca, S. Hafezian, J. Gu, B. Chakraborty, D. Ballarini, L. Martinu, V. Menon, D. Sanvitto, S. Kéna-Cohen, *Nat. Nanotechnol.* **2018**, *13*, 906.